ACS SENSORS

pubs.acs.org/acssensors

Article

Nelle, a Genetically Encoded Indicator for Branched-Chain Amino Acids Based on mNeonGreen Fluorescent Protein and LIVBP Protein

Aysilu N. Asanova, Oksana M. Subach, Sofya A. Myachina, Marta A. Evteeva, Natalia M. Gunitseva, Anna A. Borisova, Maksim V. Patrushev, Anna V. Vlaskina, Alena Yu. Nikolaeva, Lina Yang, Azat Gabdulkhakov, Elizaveta Dronova, Valeriya R. Samygina, Xian Xiao, Hu Zhao, Kiryl D. Piatkevich,* and Fedor V. Subach*

Cite This: *ACS Sens.* 2024, 9, 5135−5147

Read Online

ACCESS | Metrics & More | Article Recommendations | Supporting Information

ABSTRACT: Branched-chain amino acids (BCAAs) play an important role in the functioning of mammalian cells and the central nervous system. However, available genetically encoded indicators for BCAAs are based on Förster resonance energy transfer and have a limited dynamic range. We developed a single fluorescent protein-based sensor for BCAAs, called NeIle, which is composed of circularly permutated mNeonGreen protein inserted into the leucine-isoleucine-valine binding protein (LIVBP) from *Escherichia coli* bacteria. In solution, the NeIle indicator displayed a positive fluorescence response to adding isoleucine, leucine, and valin amino acids with high $\Delta F/F$ dynamic ranges of 27-, 19-, and 11-fold and the corresponding affinity values of 5.0, 2.9, and 75 mM, respectively. The spectral and biochemical properties of the NeIle indicator were characterized in solution. We characterized the brightness of the NeIle indicator in living mammalian cells, including cultured neurons. Using the NeIle indicator, we successfully visualized the dynamics of isoleucine transients in different organelles of mammalian cells. We obtained and analyzed the X-ray crystal structure of the NeIle indicator in an isoleucine-bound state. Structure-guided directed mutagenesis of the NeIle indicator revealed the basis of its fluorescence response and selectivity to isoleucine.

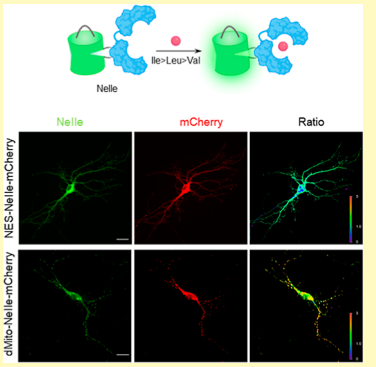

KEYWORDS: *amino acid-binding proteins, LivJ, LIVBP, INDICATOR for isoleucine, NeIle*

Real-time detection and visualization of essential amino acids in living cells are important for industrial production in agriculture and the food industry, as well as for research in cell biology and neurobiology.[1] Among essential amino acids, valine, leucine, and isoleucine are referred to as branched-chain amino acids (BCAAs).

The production of BCAAs occupies an important place in the world's chemical industry. The annual demand for BCAAs used in feed additives and pharmaceutical products is very high.[2] Genetically engineered bacterial strains are used to produce BCAAs.[3] In order to develop BCAA superproducing strains, it is necessary to monitor such amino acids at the cellular level.

The BCAAs play the role of the substrates for protein synthesis and participate in the regulation of protein, glucose, energy metabolism, and brain function.[4] BCAAs can indirectly modulate the synthesis and release of the aromatic amino acid-derived neurotransmitters.[1] Furthermore, BCAAs are significant contributors to de novo glutamate synthesis in the central nervous system (CNS). High concentrations of BCAAs are neurotoxic, resulting in increased excitotoxicity and oxidative stress. Each BCAA has its own targeted functions; for example, isoleucine has been found to be responsible for the production of β-defensins and fighting bacterial infections, leucine regulates lymphocyte activation and function, and valine controls the production of pro- and anti-inflammatory cytokines.[2] However, studies revealing the role of the BCAAs in the functioning of mammalian cells and CNS are limited by the absence of appropriate tools. Developing fluorescent genetically encoded amino acid indicators (GEAIs) would be desirable for these aims.

So far, several Förster resonance energy transfer (FRET)-based GEAIs have been produced.[1,5−7] Among them are FLIP-LivJ, FLIP-cpLivJ261, or a series of GEAIs, which are composed of LivJ or LIVBP periplasmic binding protein from *Escherichia coli* as the amino acid binding domain and the ECFP/Venus FRET pair of fluorescent proteins. The affinity of these sensors for leucine and isoleucine varied in the range of 0.15−411 μM. These sensors were used to detect variations of BCAAs in solution and in vitro in bacterial and yeast cells.

Received: May 3, 2024
Revised: September 17, 2024
Accepted: September 27, 2024
Published: October 14, 2024

https://doi.org/10.1021/acssensors.4c01055
ACS Sens. 2024, 9, 5135−5147

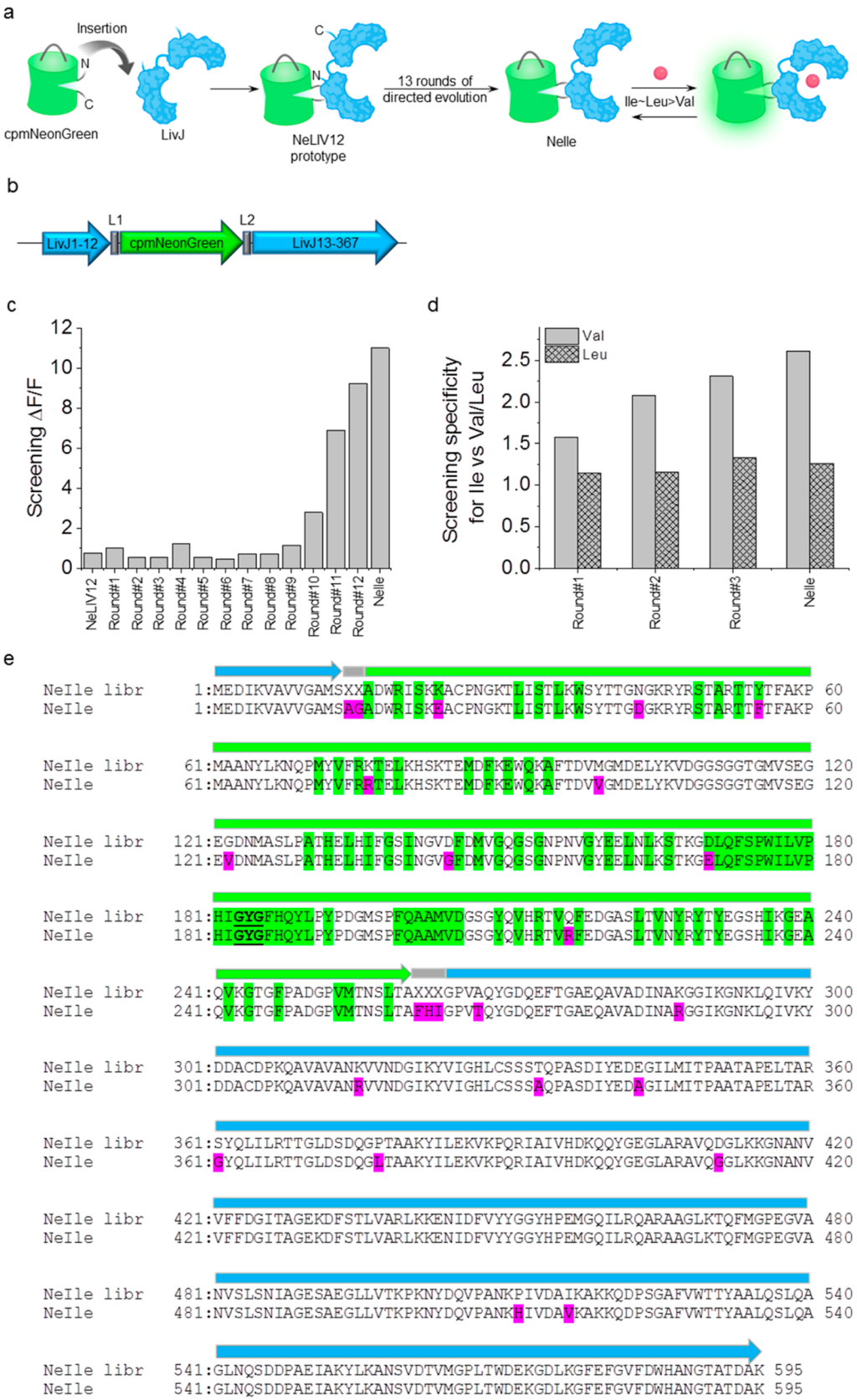

Figure 1. Development of the NeIle biosensors. (a) Schematic diagrams depicting the strategy of the NeIle design and development (created in BioRender). (b) Schematic of the annotated NeIle gene. (c) Screening $\Delta F/F$ for the top variants of the sensor from each round of directed evolution. (d) Screening Ile vs Val/Leu specificity of the top variants of the sensor from each round of directed evolution [specificity presented as the ratio of $\Delta F/F$(Ile) to $\Delta F/F$(Val/Leu)]. (e) Amino acid sequence alignment for the original library (NeIle libr) and the NeIle isoleucine indicator after 13 rounds of random mutagenesis. Amino acid residues buried inside the β-barrel are highlighted in green. Mutations and linkers are highlighted in pink. The chromophore is highlighted in bold font and underlined.

https://doi.org/10.1021/acssensors.4c01055
ACS Sens. 2024, 9, 5135−5147

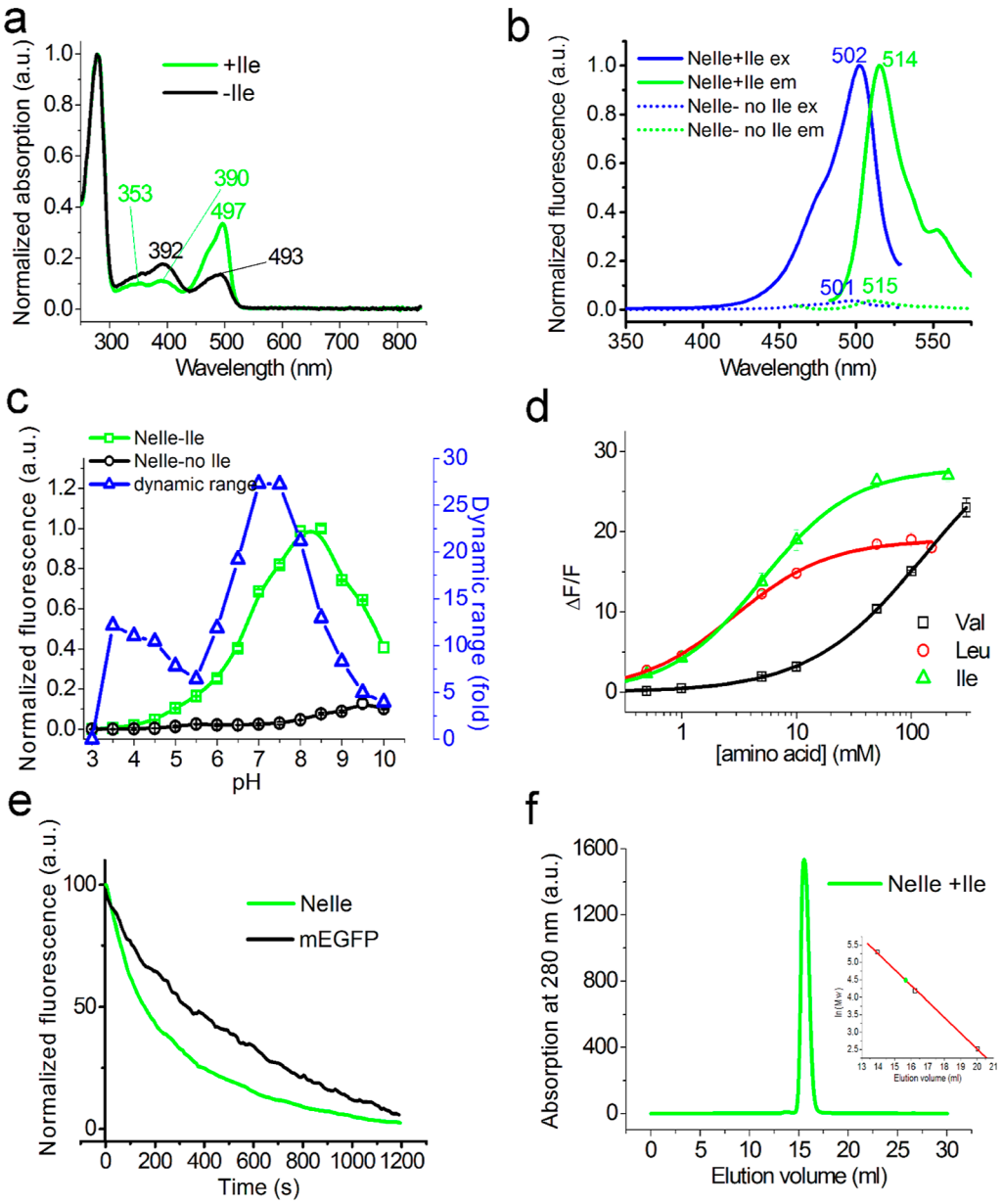

Figure 2. Properties of the NeIle indicator on purified protein in vitro. (a) Absorption spectra for NeIle protein in the absence (black curve) or presence (green curve) of 50 mM isoleucine in PBS buffer at pH 7.40. (b) Excitation and emission spectra for NeIle protein in the absence (dashed lines) or presence (solid lines) of 50 mM isoleucine in PBS buffer at pH 7.40. (c) Fluorescence intensity for NeIle protein in the absence (black curve) or presence (green curve) of isoleucine as a function of pH. Data from three replicates were averaged for analysis. Error bars represent standard deviation. (d) Dependencies of NeIle fluorescence on the concentration of isoleucine (green curve), leucine (red curve), or valine (black curve) in the buffer A 30 mM MOPS, 100 mM KCl, pH 7.3. (e) Photostability of NeIle in the presence of 23 mM isoleucine under continuous wide-field imaging using a mercury lamp (9 mW/cm^2 470/40BP light power in front of the objective). (f) Fast liquid chromatography of the NeIle protein in the presence of isoleucine. NeIle was eluted in 20 mM Tris−HCl (pH 7.80), 200 mM NaCl, and 50 mM Ile buffer. The molecular weight of NeIle was calculated by linear regression of the dependence of the logarithm of control molecular weights on the elution volume.

However, such FRET indicators have limited fluorescence response to amino acid addition in the range of 0.14−0.56 and require expensive equipment for FRET signal detection.

In the present work, using directed molecular evolution, we developed a GEAI for the BCAAs, such as isoleucine, leucine, and valine, based on mNeonGreen fluorescent protein and LIVBP protein, named NeIle. The purified NeIle protein increased its green fluorescence in response to the addition of isoleucine, leucine, and valine with $\Delta F/F$ contrasts of 27-, 19-, and 11-fold, respectively. NeIle properties were characterized in vitro. Using NeIle, we successfully visualized BCAAs or isoleucine transients in different compartments of mammalian cells, including cultured hippocampal mouse neurons. We obtained and analyzed the X-ray crystal structure of the NeIle indicator in an isoleucine-bound state.

RESULTS

Development of Genetically Encoded Green Indicator for the BCAAs. The existing FRET-based biosensors for BCAAs are characterized by a limited fluorescence dynamic range, and their imaging requires specialized filter sets.[5,6] Furthermore, these available sensors for BCAAs are unsuitable

https://doi.org/10.1021/acssensors.4c01055
ACS Sens. 2024, 9, 5135−5147

for the selective detection of individual BCAAs due to low specificity. In contrast to FRET sensors, single FP-based biosensors typically exhibit large functional changes in fluorescence intensity, which can be easily detected using a single channel on conventional imaging systems.[8] Due to the robust and easy-to-record response, single FP-based biosensors are quickly gaining popularity in neuroscience, microbiology, synthetic biology, and cell and plant biology.[9] However, single FP-based sensors for BCAAs are not currently available. Therefore, we decided to engineer a single FP-based biosensor for BCAAs with a large dynamic range and high brightness, which can enable straightforward real-time imaging in live cells. In addition, we sought to improve the selectivity of the designed sensor for a particular BCAA by using a directed molecular evolution approach.

There are two basic molecular designs of single FP-based sensors: (i) insertion of circularly permutated FP (cpFP), also referred to as reporting moiety, into a sensing domain;[10] (ii) insertion of the sensing domain into FP.[11,12] As a sensing domain, we chose to use the bacterial periplasmic LIVBP domain (aka LivJ) protein from *E. coli* as a binding domain, which was previously utilized in FRET-based sensor development.[5−7] As a reporting moiety, we used the bright green FP mNeonGreen, which was already successfully employed for many single FP-based biosensors characterized by high fluorescence dynamic range.[11,12] As the major principle of fluorescence modulation is the propagation of conformational changes from the sensing moiety upon ligand binding to the reporting moiety, the rational design of single FP-based biosensors heavily relies on the identification of the insertion sites that undergo the largest spatial shifts. We analyzed the available crystal structures of the LIVBP protein in both the ligan-bound and ligand-unbound states[13] to locate three insertion sites, namely, Ser12-Gly13, Cys53-Asp54, and Gly178-Glu179 (amino acid numbering follows that of the LIVBP protein) that undergo the largest spatial shifts upon ligand binding. Following design (i), we generated three libraries by inserting cpmNeonGreen between the determined residues and randomizing the amino acid linkers (Figure S1). In addition, following design (ii), we obtained a library with randomized linkers between a split version of the mNeonGreen protein and a circular-permutated version of the circular-permutated version of the LIVBP protein, cpLIVd (Figure S1). The cpLIVd was similar to that used in the FRET sensor FLIP-cpLivJ261 with a FRET signal change by 25% and an affinity to isoleucine >1.1 mM[6]. The split version of mNeonGreen was used from NCaMP7, the bright calcium indicator.[12] Screening of the libraries in *E. coli* resulted in the identification of functional variants based on design (i), but no functional variants for design (ii). Quantitative assessment of the functional variants revealed the best sensor prototype in the NeLIV12 library, which was characterized by a contrast of 78% and an affinity to valine of about 2 mM, and therefore, it was selected for further optimization (Figure 1a,b).

Next, we performed nine rounds of directed molecular evolution to improve the brightness and dynamic range of the sensor prototype (Figure 1c; see Methods for screening details). Since each BCAA has its own target functions,[2] it is necessary to create sensors for each of the individual BCAA. With this aim, we decided to enhance its specificity to Ile by screening random libraries with all three BCAAs and selecting variants that exhibited a higher $\Delta F/F$ ratio for Ile than for Val and Leu. After four rounds of evolution, specificity for Ile vs Val and Leu was increased by 65% and 11%, respectively, compared to the starting mutant (Figure 1d). As a final result, we selected a variant with an 11-fold fluorescent increase (on bacterial lysate) in response to isoleucine, which was 2.6- and 1.3-fold higher than those of valine and leucine (Table S1). Since the final selected variant showed the largest response to the isoleucine, it was named NeIle, and we characterized the properties of the NeIle indicator in the presence of isoleucine in more detail below.

We analyzed the amino acid sequence of the developed NeIle indicator (Figure 1e). NeIle contained 9 mutations in the cpmNeonGreen domain; three of them, K23E, Y55F, and D170E, were internal to the β-barrel and thus could affect the brightness and dynamic range of the indicator. The BCAA-binding domain contained 10 amino acid mutations that might affect the affinity and specificity of NeIle for amino acids. Thus, a single FP-based green fluorescent indicator for BCAAs (isoleucine, leucine, and valine) was developed using the directed molecular evolution in a bacterial system.

Characterization of the NeIle Indicator in Solution. First, we characterized the spectral properties and molecular brightness of the developed NeIle indicator in PBS at neutral pH 7.4 (Figure 2 and Table 1). NeIle, in the presence of isoleucine, had absorption/excitation/emission peaks at 497/502/514 nm, respectively (Figure 2a−b and Table 1), which is characteristic for deprotonated anionic form of the GFP-like

Table 1. Properties of the NeIle Indicator in Solution

properties			NeIle	mEGFP
absorption/excitation/emission maxima (nm)		−Ile	392, 493/501/515	488/ND/507
		+Ile	497/502/514	
quantum yield[a]	anionic form	−Ile	0.040 ± 0.004	0.70
		+Ile	0.47 ± 0.02	NA
	protonated form	−Ile	0.020 ± 0.004	NA
		+Ile	0.020 ± 0.002	NA
ε (M^{-1} cm^{-1})[b]		−Ile	(11,000)	53,300
		+Ile	44,000 ± 1 (26,000)	
brightness vs mEGFP (%)[c]			55	100
$\Delta F/F$ (in the presence of 50 mM amino acid)		Val	10.5 ± 1.4	NA
		Leu	19 ± 1	NA
		Ile	27 ± 1	NA
K_d (mM)		Val	≥128.1 ± 5.4	NA
		Leu	2.9 ± 0.2	NA
		Ile	5.0 ± 0.2	NA
pK_a		−Ile	8.29 ± 0.02	5.83 ± 0.04
		+Ile	6.68 ± 0.02	ND
maturation half-time (min)			5.2	14
photobleaching half-time (s)			153 ± 3	530

[a]Quantum yields (QY) for the anionic and protonated green forms were determined relative to mEGFP (QY 0.7) and mTagBFP2 (QY 0.64),[21] respectively. [b]The extinction coefficient for the anionic green form of NeIle was determined by the alkaline denaturation method. The extinction coefficients for the anionic form of NeIle shown in the brackets were calculated according to the extinction coefficient of the NeIle protein at 280 nm (equal to 77,365 M^{-1} cm^{-1}). [c]Brightness was calculated as the product of quantum yield and extinction coefficient relative to the brightness of mEGFP protein (QY 0.7 and extinction coefficient 53,300 M^{-1} cm^{-1}).

https://doi.org/10.1021/acssensors.4c01055
ACS Sens. 2024, 9, 5135−5147

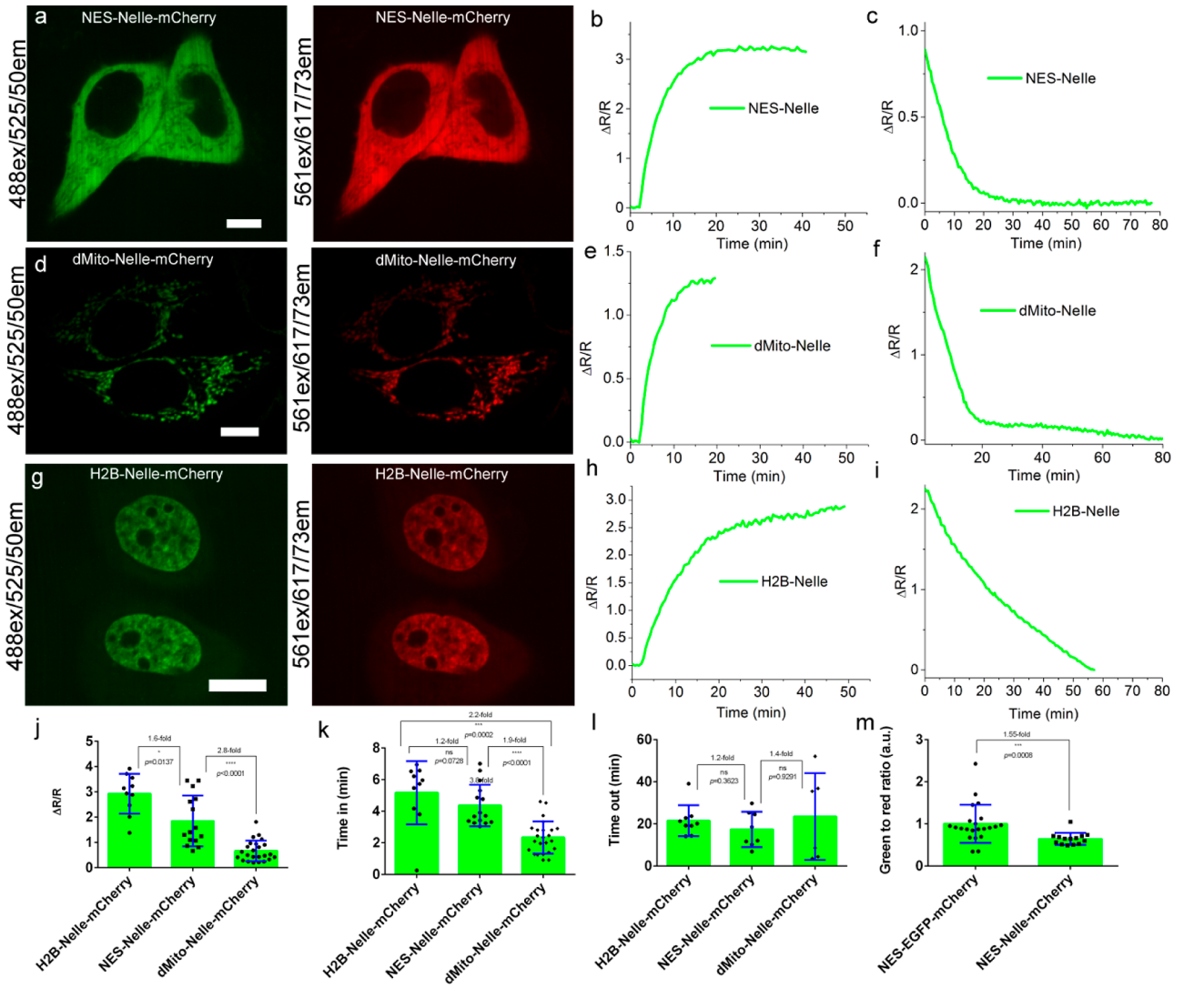

Figure 3. Brightness of NeIle and visualization of isoleucine transients in HeLa cells at room temperature. (a,d,g) Confocal images of HeLa cells expressing NES-NeIle-mCherry in the cytosol (a), dMito-NeIle-mCherry in mitochondria (d), and H2B-NeIle-mCherry in the nucleus (g) were acquired using an Andor confocal spinning-disk microscope equipped with 488 and 561 nm lasers. Images in the green and red channels are shown. Scalebar, 10 μm. (b,e,h) Dependence of ΔR/R response of NeIle-mCherry over time upon addition of 20 mM isoleucine at 2 min 10 s. (c,f,i) Dependence of ΔR/R response of NeIle-mCherry over time upon washing out of 20 mM isoleucine at 0 min. (j) Averaged ΔR/R values for NeIle-mCherry response upon addition of 20 mM isoleucine. (k) Half-times of NeIle-mCherry green-to-red fluorescence ratio changes in the nucleus, cytosol, and lumen of the mitochondria of HeLa cells upon addition of 20 mM isoleucine. (l) Half-times of NeIle-mCherry green-to-red fluorescence ratio changes in the nucleus, cytosol, and lumen of the mitochondria of HeLa cells upon washing out of the 20 mM isoleucine. (m) Brightness of the NeIle (22 cells, 3 cultures) and EGFP (14 cells, 2 cultures) proteins in the cytosol of HeLa cells were normalized to the brightness of the mCherry protein coexpressed in the same cell. HeLa cells transiently expressed NES-NeIle-mCherry or NES-EGFP-mCherry under the control of the CAG promoter.

chromophore.[14] Small peaks with absorption maxima at 353 and 390 nm were also present in the absorption spectrum. In the absence of isoleucine, the absorption spectrum exhibited two peaks at 392 and 493 nm in a ratio of 1.15:1, corresponding to the protonated and anionic forms of the GFP-like chromophore.[14] The quantum yield of the anionic form decreases by a factor of 12 in the absence of isoleucine. The protonated form in the absence and presence of isoleucine did not fluoresce (quantum yield of 0.02). The molecular brightness for the designed NeIle indicator in the presence of isoleucine, calculated as the product of the extinction coefficient and quantum yield, was 1.8 times lower than the brightness for mEGFP (Table 1). Thus, the increase in green fluorescence in the presence of isoleucine is due to a greater quantum yield and a greater amount of the anionic form of the chromophore.

Since pH varies in cellular organelles from 4.5 in lysosomes to 8.0 in mitochondria,[15] the pH stability of the NeIle indicator is an important property for functional imaging of subcellular structures in living cells. We evaluated the pH dependence of NeIle indicator fluorescence in the pH range from 3.0 to 10.0 (Figure 2c and Table 1). NeIle in the isoleucine-bound state had a pK_a value of 6.68. In the absence of isoleucine, pK_a increased to 8.29. A similar difference in pK_a was observed for the two states of many genetically encoded fluorescent calcium indicators; for example, in the case of the green calcium indicator GCaMP6s, calcium ion binding resulted in a decrease in pK_a from 9.6 to 6.2 (ref 16), and in the case of the red

https://doi.org/10.1021/acssensors.4c01055
ACS Sens. 2024, 9, 5135−5147

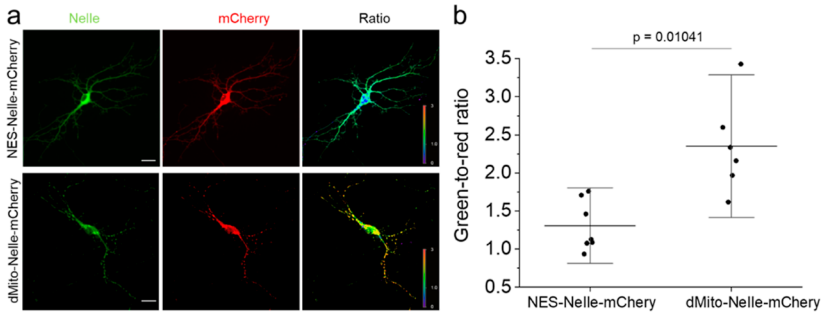

Figure 4. Expression of NeIle in cultured mouse neurons. (a) Representative fluorescence and ratio images of cortical neurons expressing NES-NeIle-mCherry and dMito-NeIle-mCherry, respectively (scale bar = 20 μm) (b) Ratio of NeIle fluorescence intensity to mCherry fluorescence intensity. The scatter interval plot is used: middle horizontal line, mean; top and bottom horizontal lines, 25% and 75% percentiles for the data; whiskers extend 1.5× the interquartile range from the 25th and 75th percentiles. One sample *t*-test was performed.

calcium indicators FRCaMP and R-GECO1, from 8.9 to 6.6 (ref 17).

We then measured the affinity and fluorescence dynamic range of the NeIle indicator for three amino acids: valine, leucine, and isoleucine. The highest affinity was observed for leucine with the K_d value of 2.9 ± 0.2 mM, which was 1.7-fold higher than that for isoleucine with K_d of 5.0 ± 0.2 mM (Table 1). In turn, the affinity for valine was 26-fold lower than that for leucine. However, the fluorescence response to isoleucine was characterized by a large $\Delta F/F$ of 27-fold vs only 10.5 ± 1.4 for Val and 19 ± 1 for Leu (Table 1). Considering both the binding curves and the amplitude of the $\Delta F/F$ fluorescence response, at low amino acid concentrations of up to 3 mM, isoleucine had approximately equal fluorescence to leucine but superior to valine, and at higher concentrations, isoleucine fluorescence was superior to both amino acids (Figure 2d). Thus, NeIle was more beneficial at detecting isoleucine and leucine than valine.

To further evaluate the performance of NeIle, we characterized other biochemical and photochemical properties, including the maturation rate, photostability, and oligomeric state (Table 1). The maturation rate of NeIle at 37 °C was 2.7-fold faster than the maturation rate of mEGFP. In single-photon mode under continuous wide-field illumination using a suspension of microdroplets in oil under continuous illumination with a metal halide lamp using 470/40 nm light and a 63× magnification oil objective, the photostability of mEGFP was 3.5-fold higher than the photostability of NeIle (Figure 2e). Since the monomeric state of an indicator ensures its low cytotoxicity and ability to label proteins and organelles in mammalian cells, we also characterized the oligomeric state of the developed NeIle indicator using fast protein liquid chromatography (FPLC; Figure 2f). NeIle was eluted as a monomer on FPLC. Hence, the NeIle indicator is a monomer and can be used for protein labeling. Thus, the NeIle indicator is the first monomeric genetically encoded green fluorescent indicator for isoleucine (and to a lower extent for leucine and valine) with a molecular brightness of 55% of that of mEGFP and fluorescent response to isoleucine addition of 27, and the dissociation constant of 5 mM; NeIle is more pH-sensitive than mEGFP; it matures 2.7-fold faster than mEGFP, but it is 3.5 times less photostable than mEGFP.

Visualization of the NeIle Indicator in Different Organelles of Mammalian Cells. To test how the NeIle indicator localized in different compartments of cultured mammalian cells, we expressed NeIle in the cytosol, mitochondria, nucleus, and plasma membrane of HeLa cells (Figure S2). As can be seen, the indicator for BCAAs correctly localizes to all parts of mammalian cells and does not interfere with cell function, as shown by the presence of different phases of cell division expressing NeIle fusion proteins with nuclear H2B protein (Figure S2). This confirms the FPLC data for the monomeric state of NeIle.

We also generated the ratiometric version of the NeIle indicator, assessed its localization in different organelles, and estimated the relative physiological concentrations of BCAAs in different organelles of mammalian cells. To this end, we created a NeIle fusion protein with the red fluorescent protein mCherry and targeted it to the cytosol, mitochondria, and nucleus (Figure 3a,d,g). We then calculated the ratio of NeIle green fluorescence to mCherry red fluorescence $F_g/F_r = R$ (Figure S3). This ratio was about the same in the cytosol and in the nucleus. However, it was 1.6- and 1.4-fold higher in mitochondria than in the cytosol and nucleus, respectively. Since the NeIle indicator bound to BCAAs was brighter than that without amino acids, the R ratio of green to red fluorescence should be higher at the organelle's higher BCAA concentrations. However, the differences in pH in different cell organelles and the sensitivity to the pH of the NeIle indicator should still be taken into account. Consequently, the data obtained may be explained by a higher BCAA concentration in mitochondria compared to the cytosol and nucleus and/or by differences in pH in different organelles of the cell.

Next, we compared the intracellular brightness of the NeIle indicator in HeLa cells to that of commonly used EGFP. HeLa cells were transiently transfected with pAAV-CAG-NES-NeIle-mCherry or pAAV-CAG-NES-EGFP-mCherry plasmids. The brightness of the green NeIle and EGFP proteins was normalized to the brightness of the equally expressing RFP mCherry (Figure 3m). Under physiological conditions, the brightness of the NeIle indicator in the cytosol of the HeLa cells was 1.55-fold lower (p = 0.0008) than the brightness of the EGFP protein. Hence, the NeIle indicator has sufficient intracellular brightness in mammalian cells.

To further explore the applicability of NeIle in other cell types, we expressed the NeIle-mCherry sensor in the cytoplasm and mitochondria of primary mouse cultured neurons under the CAG promoter. When expressed in neurons, the green fluorescence of NeIle-mCherry was evenly distributed within the cytosol as well as individual dendrites, without any aggregation or nonspecific localization. Although the sensor was excluded from the nucleus, most likely due to the decreased passive diffusion through nuclear pores for the larger molecules (Figure 4a). In turn, the red fluorescence of

https://doi.org/10.1021/acssensors.4c01055
ACS Sens. 2024, 9, 5135−5147

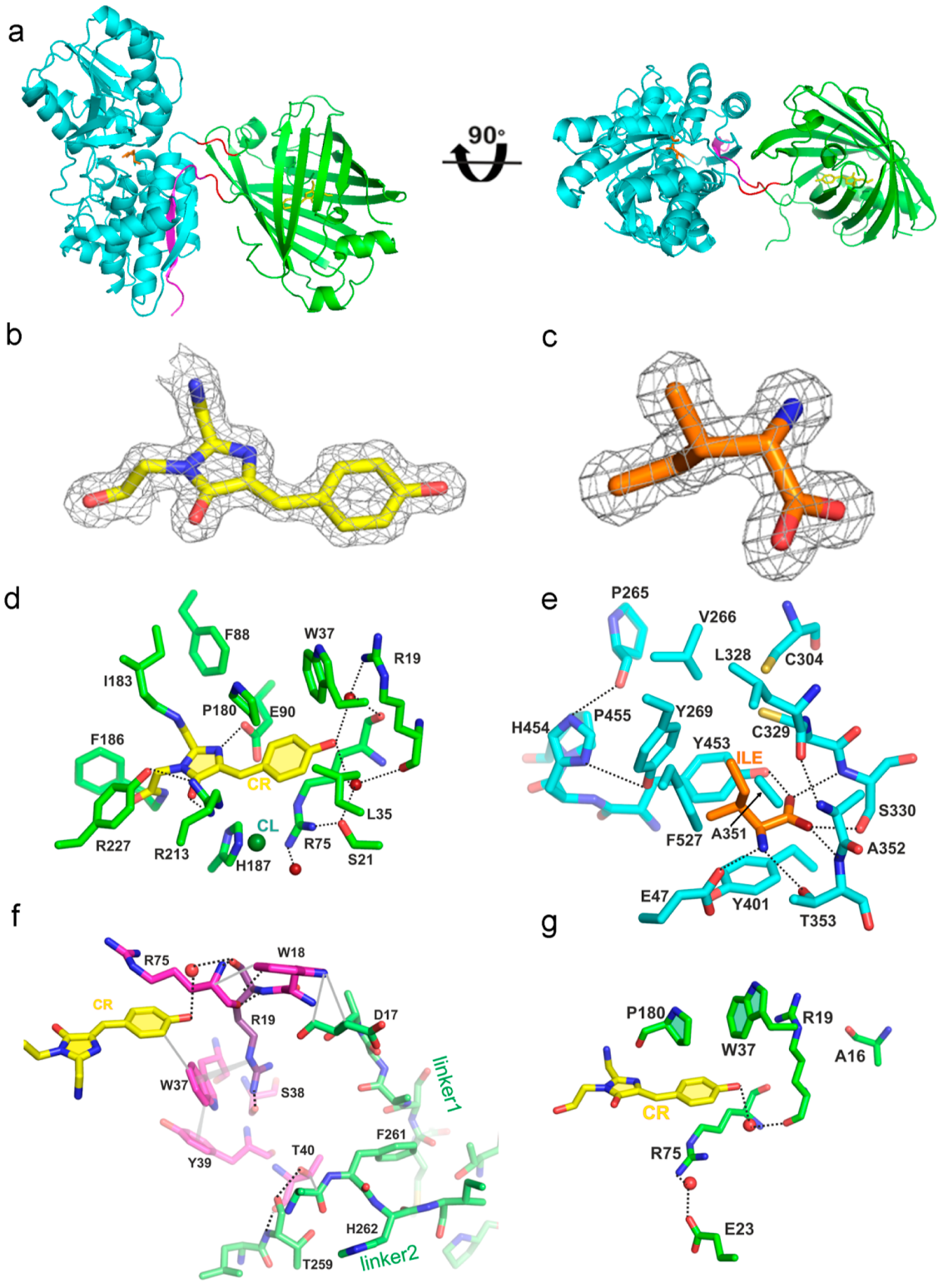

Figure 5. Crystal structure of the NeIle indicator in the isoleucine bound state. (a) Cartoon representation of the NeIle indicator structure. Fluorescent and LIVBP domains and linkers are shown in green, cyan/magenta, and red, respectively. (b,c) 2Fobs-Fcalc electron density map (gray mesh and contoured at the 1.1σ level) is shown for the chromophore (b) and isoleucine (c) of the NeIle. (d,e) Immediate 4.5 Å surrounding of the chromophore (d) and isoleucine of the NeIle indicator (e). Hydrogen bonds and water molecules are shown as green dashed lines and spheres, respectively. (f) Environment of R19 and tyrosine ring of the chromophore of NeIle. Carbon atoms of residues of the fluorescent domain are colored in magenta. Carbon atoms of chromophore and linker residues are colored in yellow and light green, respectively. H-bonds are indicated by black dash lines. Hydrophobic interactions including stacking are shown by gray lines. (g) Arrangement of A16, R19, and E23 relative to the NeIle chromophore. Interaction of R19 and E23 with the amino acid residues of the chromophore environment. Carbon atoms of the chromophore and protein are yellow and green, respectively. Water molecules are shown by red spheres. Possible H-bonds are shown by black dash lines.

https://doi.org/10.1021/acssensors.4c01055
ACS Sens. 2024, 9, 5135−5147

mCherry, while labeling the cytoplasm, exhibited bright aggregates and puncta in the soma and proximal neurites (Figure 4a). The expression of the mitochondria-targeted version of NeIle-mCherry in neurons produced stereotypic mitochondria patterns with a high degree of green and red fluorescence colocalization, as assessed by visual inspection of the images (Figure 4a). A high degree of green and red fluorescence colocalization allowed us to calculate the fluorescence ratio, which, as suggested above, can reflect the relative concentrations of BCAAs within single cells and across cellular populations. While the overall ratio within single cells was relatively consistent, we observed an almost 1.8-fold high ratio in mitochondria compared to the cytoplasm of neurons (Figure 4b). These results were consistent with the observation in HeLa cells and may indicate a higher relative concentration of BCAAs in mitochondria vs cytoplasm.

Visualization of the Isoleucine Transients in Different Organelles of Mammalian Cells Using the NeIle Indicator and Confocal Microscopy. Next, we visualized isoleucine transients in different organelles of cultured mammalian cells using the ratiometric NeIle-mCherry indicator and confocal microscopy. NeIle-L3-mCherry ratiometric version was transiently expressed in the cytosol, lumen of mitochondria, and nuclei of HeLa cells as described above. Amino acids were removed from the cells by incubation of the cells in DBPS buffer for 1−4 h at 37 °C. After the addition of the 20 mM isoleucine, we observed a gradual increase in the green-to-red ratio of the NeIle-mCherry sensor in the different organelles of the cells (Figure 3b,e,h). The average maximal $\Delta R/R$ values in the nucleus, cytosol, and mitochondria were 2.9 ± 0.8, 1.8 ± 1.0, and 0.66 ± 0.41, respectively (Figure 3j). As compared to the cytosol, the averaged maximal $\Delta R/R$ values in the nucleus and mitochondria were 1.6- larger and 2.8-fold smaller, respectively (Figure 3j). The average half-times of the green-to-red ratio increase in the nucleus, cytosol, and mitochondria were 5.2 ± 2.0, 4.4 ± 1.3, and 2.3 ± 1.1 min, respectively (Figure 3k). Hence, as compared to the cytosol, the kinetics of the green-to-red ratio increase in the nucleus and mitochondria were the same or 1.9-fold faster, respectively (Figure 3k).

After washing out extracellular isoleucine, we observed a decrease in the green-to-red fluorescence ratio of the NeIle-mCherry sensor (Figure 3c,f,i,l). The average half-times of the green-to-red ratio decrease in the nucleus, cytosol, and mitochondria were 21 ± 7, 17 ± 8, and 23 ± 21 min, respectively (Figure 3l). Hence, the kinetics of the green-to-red ratio decreases in the organelles studied were the same (Figure 3l).

Overall, using the NeIle-mCherry ratiometric sensor, we successfully studied isoleucine dynamics in different organelles of mammalian cells.

Crystal Structure of the NeIle Indicator in the Isoleucine Bound State. Next, we obtained and analyzed the crystal structure of the NeIle indicator in an isoleucine-bound state in order to understand the molecular basis of the mechanism of its fluorescence response and selectivity to isoleucine. The NeIle crystal structure was solved at 1.62 Å resolution. According to analysis of the overall 3D structure, NeIle is composed of two domains: a fluorescent domain with a typical β-barrel fold and an isoleucine-binding domain (Figure 5a). Both the GFP-like chromophore and isoleucine were clearly seen (Figure 5b,c). The isoleucine binding domain of the NeIle indicator had a similar structure as LIVBP protein in an isoleucine bound state, and the location of the isoleucine residue was the same (Figure S4); however, we observed a slight shift of two subdomains relative to each other in the NeIle sensor as compared to LIVBP protein in the isoleucine bound state. The fluorescent domain of the NeIle indicator had a structure similar to the structure of the mNeonGreen progenitor (Figure S5). Domains were joined via two flexible linkers, 12−18 (linker 1) and 259−264 (linker 2). Amino acid linkers were mainly connected by hydrophobic interactions (Figure S6).

We next analyzed the immediate 4.5 Å environment of the NeIle chromophore. The chromophore in NeIle formed 5 direct hydrogen bonds with E90, P180, R213, and Y229 and 8 water-mediated hydrogen bonds with R19, S21, R75, H187, Y209, and Y229 (Figure 5d). 4.5 Å surroundings of the chromophores of NeIle and mNeonGreen were the same except the different side chains of the residues R19 in NeIle and corresponding C139 in mNeonGreen, and L35 in NeIle and corresponding F155 in mNeonGreen (Figure S7).

To elucidate the molecular basis of the mechanism of the NeIle fluorescence response to isoleucine, we analyzed the contacts of the tyrosine hydroxyl anion of the chromophore with the surrounding amino acids (Figure 5d). These contacts might play the most important role in the mechanism of the fluorescence response of the NeIle indicator to isoleucine, as the chromophore in the absence and presence of isoleucine had a preferentially different protonation state (Figure 2a) The tyrosine hydroxyl in the isoleucine-bound NeIle was mainly in the anionic state (Figure 2a), which can be stabilized by the formation of three water-mediated hydrogen bonds with the main chain carbonyls of R19 and R75 and with the hydroxyl group of S21 (Figure 5d). NeIle also exhibits a 12-fold decrease in quantum yield upon the release of the isoleucine ligand (Table 1). We speculate that the observed decrease in quantum yield of the chromophore upon release of isoleucine could be caused by the loss of the contacts between the chromophore and the surrounding amino acids resulting in an increase in the mobility of the chromophore and its accessibility to solvent molecules. The NeIle structure showed that the LIVBP isoleucine-binding domain consisted of two subdomains. Based on the crystal structures of the LIVBP domain in the presence (PDB: 1z17) or absence (PDB: 1z15) of isoleucine, we could see a large shift of these subdomains relative to each other upon binding of isoleucine (Figure S4). According to the NeIle crystal structure, R19 was at the end of the amino acid linker between the isoleucine bound LIVBP-N-terminal β-sheet (Figure 5a, in magenta) and the fluorescent cpNeonGreen domain; R19 formed stacking interactions with W37 which had hydrophobic contact with the chromophore (Figure 5f). Furthermore, R19 had a network of interactions, including residues in the linkers in the second sphere of interactions (Figure 5f). We could suggest that upon dissociation of isoleucine from NeIle, there was a large rearrangement in the LIVBP subdomains, which resulted in a shift of R19. This, in turn, might cause weakening or disruption of the water-mediated hydrogen bond between the R19 main chain carbonyl and the chromophore tyrosine hydroxyl, leading to the protonation of the chromophore. In addition, since the R19 main chain was hydrogen bonded to the carbonyl of the R75 main chain and through the water to the hydroxyl group of the S21, displacement of R19 might rearrange R75 and S21 and disrupt the two remaining

https://doi.org/10.1021/acssensors.4c01055
ACS Sens. 2024, 9, 5135−5147

hydrogen bonds to the hydroxyl of the chromophore and favor protonation of the chromophore.

We next provided biochemical evidence of the importance of the R19 residue for the response of the NeIle indicator to isoleucine amino acid. We tested whether R19 in combination with A16 and E23 amino acid mutations in the immediate surroundings of the chromophore in the fluorescent part (Figure 5g) could change the positive response of the NeIle indicator to a negative one. Since we suggested that the fluorescence response might depend on the interaction between the fluorescent and the LIVBP isoleucine-binding domains, we chose the A16 and R19 amino acid residues that were located in the linker and near the linker between the N-part of the isoleucine-binding protein LIVBP and the mNeonGreen fluorescent part, respectively. The E23 residue was chosen because the K23E mutation appeared during the molecular evolution of the NeIle indicator and was favorable for the large positive fluorescence response of NeIle. We obtained the library with the randomized amino acids in positions 16, 19, and 23. We found that the NeIle/A16W/R19T/E23H and NeIle/A16S/R19T/E23H mutants had a negative response to isoleucine, valine and leucine (Table 2).

Table 2. Influence of Mutations in the Ile or the Chromophore Environment on Selectivity and Positive or Negative Response of Indicators

	$\Delta F/F$		
mutant	Ile	Val	Leu
NeIle	12.2	4.7	9.7
NeIle/C329L	3.9	4.9	3.4
NeIleC304I	4.5	6.3	3.7
NeIle/C304F	2.3	1.8	2.9
NeIle/V266I	6.6	2.3	7.3
NeIle/F527W	2.9	1.3	4.4
NeIle/A351S	17.7	4.1	16.3
NeIle/A16W/R19T/E23H	−0.58	−0.46	−0.33
NeIle/A16S/R19T/E23H	−0.46	−0.26	−0.37
NeIle/A16W	4.0	2.2	1.9
NeIle/A16S	4.5	2.6	2.4
NeIle/R19T	1.5	1.0	1.5
NeIle/E23H	0.5	0.4	0.6

We also tested the effect of each individual amino acid substitution on the NeIle indicator: A16W, A16S, R19T, and E23H (Table 2). The fluorescent response to isoleucine was 3−24-fold lower in these mutants compared with the NeIle indicator but still remained positive. Only the combination of changes in all three amino acids resulted in a negative response. Thus, amino acids in the fluorescent part near the chromophore and the linker are responsible for the amplitude and the sign of the response (positive or negative) to isoleucine. According to the crystal structure of the NeIle indicator, we can suggest that the amino acid at position 19 is the key residue that translates conformational changes in the LIVBP isoleucine-binding domain into fluorescence changes.

We also looked at the isoleucine environment in the NeIle indicator (Figure 4e). The carboxyl group of Ile forms three hydrogen bonds with S330, T353, and Y453. The amino group of Ile is hydrogen bonded to the A351, T353, and E477. The isoleucine side chain is in the hydrophobic environment formed by V266, Y269, L328, C329, A351, Y401, Y453, and F527.

To understand how the amino acids surrounding the isoleucine side chain affect the selectivity to isoleucine, we replaced some of these amino acids in the NeIle indicator with those with bulkier side chains and assessed the dynamic range of NeIle and its selectivity to isoleucine, valine, and leucine amino acids. We checked the selectivity of NeIle V266L, V266I, V266F, Y269W, C304V, C304L, C304I, C304F, L328W, L328F, C329X, A351X, and F527W mutants. The C304I and C329L mutants revealed higher selectivity to valine (Table 2). The V266I, C304F, and F527W variants showed higher selectivity to leucine. The A351S mutation resulted in a higher selectivity to isoleucine compared to that to valine. Therefore, mutations in the hydrophobic environment of the isoleucine side chain may adjust the selectivity of the NeIle indicator.

DISCUSSION

In this work, we developed a single FP-based fluorescence indicator for BCAAs (isoleucine, leucine, and valine) based on circularly permutated mNeonGreen fluorescent protein and LIVBP protein, characterized its properties in solution, assessed its performance in cultured mammalian cells, and uncovered the molecular basis of its functioning using its X-ray crystal structure and mutagenesis.

As compared to the existing FRET sensors for isoleucine such as FLIP-LivJ, FLIP-cpLivJ261, or series of GEAIs, which have responses to isoleucine or leucine in vitro in the range of 0.14−0.56,[5,6] the NeIle demonstrates a significantly enhanced dynamic range to isoleucine of 27 in vitro. NeIle also preserved a high dynamic range in the nucleus, cytosol, and lumen of mitochondria of mammalian cells of 2.9 ± 0.8, 1.8 ± 1.0, and 0.66 ± 0.41, respectively. In comparison to available FRET-based sensors,[5,6] NeIle has 12−33,000-fold lower affinity to isoleucine amino acid (K_d of 0.00015−0.4 mM vs K_d of 5 mM, respectively). The affinity of the NeIle indicator to isoleucine and leucine amino acids is appropriate for their detection in the cytosol of mammalian cells; the concentration of isoleucine and leucine in the cytosol of the mammalian cells in standard medium is around 0.4−2 and 0.6−2 mM, respectively,[7,18] and depends on the composition of the external medium. NeIle also outperforms FRET-based sensors in terms of a smaller molecular size and simpler signal measurements. One limitation of the NeIle indicator is its low specificity to isoleucine since NeIle also responded to leucine and, to a lesser extent, to valine amino acids.

We found that isoleucine is efficiently taken up in and excreted out of the cytosol, nuclei, and lumen of mitochondria of mammalian cells (Figure 3). This finding is in accordance with the efficient transport of isoleucine in the cytosol of the mammalian cells observed earlier and subscribed to the action of the different amino acid transport systems.[18]

Crystal structure analysis of NeIle opens the possibility of adjusting indicator specificity to individual amino acids, isoleucine, valine, or leucine and the development of the indicators for each of individual BCAAs. Found prototype of the NeIle indicator with inverted response to isoleucine opens up the possibility of developing such a type of indicator with enhanced dynamic range. Indicators for BCAAs with an inverted phenotype might facilitate the screening of super-producer strains with enhanced extracellular transport of the BCAAs.

https://doi.org/10.1021/acssensors.4c01055
ACS Sens. 2024, 9, 5135−5147

MATERIALS AND METHODS

Bacterial Vector Cloning and Mutagenesis. The LivJ gene encoding BCAA-binding protein LIVBP was found in bacteria from the VKPM B-13692 collection and cloned into the pUC119 vector and sequenced. The sequence of the LivJ gene is shown in Figure S8. The genes of the designed indicator prototypes were cloned in the pBAD/HisB plasmid (Invitrogen) at *Bgl*II/*Eco*RI restriction sites using the primers listed in Table S2. Indicators were expressed in BW25113 bacterial cells (kindly provided by Verkhusha V.V. from Albert Einstein College of Medicine, New York, USA).

Randomized amino acid indicator libraries were obtained by PCR in the presence of Mn^{2+} ions (according to the Diversify PCR Random Mutagenesis Kit User Manual, Clontech, introducing 2−3 random mutations per 1000 base pairs) and cloned by *Bgl*II/*Eco*RI restriction sites into pBAD/HisB plasmid DNA.

Bacterial Libraries Screening. Bacterial libraries were screened on Petri dishes under a fluorescence microscope. Briefly, the expression of green sensors in colonies on Petri dishes was induced by 0.0002% arabinose for 24 h at 37 °C. About 10,000 colonies of a bacterial library expressing sensor variants were screened on Petri dishes under a Leica M205FA fluorescent stereomicroscope (Leica, Germany) equipped with a DFC310FX camera (Leica Microsystems, Germany) and an EL6000 mercury−metal halide light source (Leica Microsystems, Germany). Since bacterial cells contain amino acids, colonies with maximum fluorescence in the green channel (excitation at 480/40 nm and emission at 535/40 nm) were selected for screening on Petri dishes. Then, using a 96-well plate and Plate reader, we analyzed the top 50−70 clones in the bacterial lysates. For this purpose, 5−10 μL of lysate was added to 200 μL of 30 mM MOPS, pH 7.20, and 100 mM KCl buffer containing 0 and 50 mM valine, leucine, or isoleucine to assess contrast and specificity to the amino acid. 1−2 clones were selected for maximal contrast and specificity to isoleucine.

Purification and Characterization of Proteins In Vitro. To characterize the spectral properties in vitro, proteins were purified from 250 mL of LB medium supplemented with ampicillin (100 μg/mL) and arabinose (0.004%) and grown overnight at 37 °C, 220 rpm. Cells were precipitated at 5000*g* for 10 min. The precipitate was then resuspended in 10 mL of PBS, 100 mM NaCl, and 10 mM imidazole, pH 7.40. Cells were disrupted by sonication for 4 min at 20% power. The cell lysate was separated from the cell debris by centrifugation at 18,000*g* for 10 min. The protein was then bound to 500 μL of Ni-NTA resin (1:1 suspension) for 1 h at 4 °C. After washing the resin 3 times with 5 mL of PBS, 100 mM NaCl, and 10 mM imidazole, pH 7.40, we performed protein elution in 400 μL of PBS buffer supplemented with 400 mM imidazole, 100 mM NaCl, pH 7.40. Proteins were dialyzed at 4 °C for 24 h opposite 1 L of buffer A 30 mM MOPS, 100 mM KCl pH 7.30.

Extinction coefficients were determined by alkaline denaturation, assuming that the GFP-like chromophore in 1 M NaOH has an extinction coefficient of 44,000 M^{-1} cm^{-1}. Absorption spectra were recorded using a NanoDrop 2000 (USA).

QY of NeIle protein in 30 mM MOPS, 100 mM KCl, pH 7.30 in the absence of isoleucine and in the presence of 50 mM isoleucine were determined relative to the mEGFP protein in PBS buffer used as reference standard with a QY equal to 0.7. Proteins were diluted to get absorption at 470 nm equal to 0.05, 0.04, 0.03, 0.02, and 0.01 values, and emission spectra were recorded in the range of 480−700 nm. Then, the tangents of the slope (tgα) of the curve of dependence of the integrated fluorescence values in the range of 480−700 nm on the absorbance at 470 nm were calculated, and the quantum yield was calculated according to the following equation: $QY = 0.70 \times \frac{tg\alpha_{NeIle}}{tg\alpha_{mEGFP}}$. The fluorescence spectra were measured by using a CM2203 spectrofluorometer (Solar, Belarus).

To study protein maturation, BW25113 bacteria carrying the pBAD/HisB-NeIle or pBAD/HisB-mEGFP plasmids were grown in 20 mL of LB medium supplemented with ampicillin at 37 °C overnight. To induce protein expression, 0.2% arabinose was added, and bacterial cultures were incubated at 37 °C in 15 mL tubes filled to the brim and tightly sealed to restrict oxygen access. After 2 h, the cultures were centrifuged at 3500 rpm for 12 min, and the cell pellet was resuspended in 800 μL of PBS, chloramphenicol (mEGFP) or 30 mM MOPS, 100 mM KCl, pH 7.3, 50 mM isoleucine, chloramphenicol (NeIle) buffer. The cell suspension was sonicated for 40 s at 20% power and centrifuged at 20,000*g* for 2 min 100 μL of protein aliquot was transferred into a prewarmed quartz cuvette with 2.9 mL of PBS, chloramphenicol (mEGFP) or 30 mM MOPS, 100 mM KCl, pH 7.3, 50 mM isoleucine, chloramphenicol (NeIle) buffer, and protein maturation was registered at 37 °C by green fluorescence changes monitored using a CM2203 spectrofluorometer (Solar, Belarus).

Size-exclusion chromatography was performed using a Superdex™ 75 10/300 GL column and a GE AKTA Explorer (Amersham Pharmacia, UK) FPLC System.

For K_d titrations, NeIle protein (50 nM final concentration) was mixed with 200 μL of buffer A supplemented with 0, 0.1, 0.2, 0.5, 1, 5, 10, 50, and 100 (valine, leucine), 150 (leucine), 208 (isoleucine), 300 (valine) mM isoleucine, valine, or leucine. After incubation at room temperature for 20 min, the green fluorescence was recorded using Modulus II Microplate Reader (TurnerBiosystems, USA). K_d values and Hill coefficients for amino acids binding by NeIle sensor were calculated by nonlinear regression of experimental points by the Hill equation: $I = I_{max}\frac{[Cd^{2+}]^n}{K_d^n + [Cd^{2+}]^n}$, where I is the fluorescence intensity at a particular amino acid concentration and I_{max} is the fluorescence intensity at saturating cadmium ion concentrations.

Proteins were photobleached in suspension of purified protein in mineral oil using a Zeiss Axio Imager Z2 microscope (Zeiss, Germany) equipped with a 120 W mercury short-arc lamp (LEJ, Germany), a 63 × 1.4 NA oil immersion objective lens (PlanApo, Zeiss, Germany), a 470/40BP excitation filter, a FT 495 beam splitter, and 525/50BP emission filters. Light power density (64 mW/cm^2) was measured at the rear focal plane of the objective lens using a PM100D power meter (ThorLabs, Germany) equipped with an S120VS sensor (ThorLabs, Germany). 1.5 μL of protein in water buffer was thoroughly mixed with 10 μL of mineral oil and placed between slide glass and a cover glass. The NeIle sensor (50 μM) was bleached in a 5.4:4.6 mixture of PBS buffer and 30 mM MOPS, 100 mM KCl, and 50 mM isoleucine buffer. mEGFP (50 μM) was photobleached in a PBS buffer.

Mammalian Plasmid Construction. In order to construct the pAAV-*CAG*-NES-NeIle plasmid, the NeIle gene was PCR-amplified as the *Bgl*II-*Eco*RI fragment and swapped with the mCherry gene in the pAAV-*CAG*-NES-mCherry vector.

In order to construct the pAAV-*CAG*-dMito-NeIle and pAAV-*CAG*-H2B-NeIle plasmids, the NeIle gene was PCR-amplified as the *Bgl*II-*Hin*dIII fragment and swapped with the mCherry and B-GECO1 genes in the pAAV-*CAG*-*d*Mito-mCherry and pAAV-*CAG*-H2B−B-GECO1 vectors, respectively.

In order to construct the pAAV-CAG-Igk-NeIle-TM plasmid, the NeIle gene was PCR-amplified as the *Bgl*II-SpeI fragment and swapped with the iGluSnFR gene in the pAAV-CAG-Igk-iGluSnFR-TM vector.

In order to construct the pBAD/Myc-HisB-NeIle-L3-mCherry plasmid, the NeIle gene was PCR-amplified as a *Bgl*II-*Eco*RI fragment and swapped with the mTagBFP gene in the pBAD/Myc-HisB-mTagBFP-L3-mCherry vector.

In order to construct the pAAV-CAG-NES-NeIle-L3-mCherry, pAAV-CAG-dMto-NeIle-L3-mCherry, and pAAV-CAG-H2B-NeIle-L3-mCherry plasmids, the NeIle-L3-mCherry gene was PCR-amplified as a *Bgl*II-SpeI fragment and swapped with the NeIle gene in the pAAV-*CAG*-NES-NeIle, pAAV-*CAG*-dMito-NeIle, and pAAV-*CAG*-H2B-NeIle vectors, respectively.

The mammalian plasmids generated in the course of this study and corresponding full plasmid nucleotide sequences are available from the WeKwikGene plasmid repository at Westlake Laboratory, China (https://wekwikgene.wllsb.edu.cn/).

Cell Culture and Transfection. HeLa Kyoto cells were maintained in Dulbecco's Modified Eagle Medium (GIBCO)

https://doi.org/10.1021/acssensors.4c01055
ACS Sens. 2024, 9, 5135−5147

supplemented with 10% fetal bovine serum (FBS) (Sigma), 2 mM GlutaMax-I (GIBCO), 50 U/ml penicillin, and 50 μg/mL streptomycin (GIBCO). Plasmids for transfection were prepared using a Plasmid Miniprep purification kit (Evrogen, Russia). Transfection was performed using TurboFectTM (Thermo Fisher Scientific, USA) according to the manufacturer's protocol.

Mammalian Live-Cell Imaging. HeLa Kyoto cell cultures were imaged 48−72 h after transfection using an Andore confocal microscope equipped with an inverted Nikon Eclipse Ti microscope, a 75 W mercury−xenon lamp (Hamamatsu, Japan), a 60× oil immersion objective (Nikon, Japan), a 16-bit QuantEM 512SC electron-multiplying CCD (Photometrics, USA), and a cage incubator (Okolab, Italy). For time-lapse imaging experiments, cells were visualized after incubation in DPBS buffer at 37 °C, with 5% CO_2 for 1−4 h. 20 mM isoleucine was added at 2.1 min after the start of imaging at room temperature. In 0.5−1.5 h after 20 mM isoleucine addition, it was washed out with DPBS buffer, and cells were imaged for 1−2 h at room temperature.

Culture and Imaging in Primary Neurons and Astrocytes. All animal maintenance and experimental procedures for mice were conducted according to the Westlake University animal care guidelines, and all animal studies were approved by the Institutional Animal Care and Use Committee of Westlake University under animal protocol no. 19-044-KP-2. Cortical astrocytes and hippocampal neurons were harvested from postnatal day 0 C57BL/6 pups, without the distinction of sex, obtained from the Animal Facility at Westlake University. Dissected brain tissues were digested using 0.25% Trypsin−EDTA (YEASEN Biotech, China) for 10 min at 37 °C, a process that was subsequently halted by the addition of advanced medium (Gibco, USA) containing 10% FBS (Gibco, USA). The dissociated neurons were plated on 14 mm coverslips (Biosharp, China) precoated with Matrigel (Animal Blood Ware, China). Neuronal cultures were maintained in Neurobasal-A medium (Gibco, USA) supplemented with 10% FBS (Gibco, USA) and 2% B27 supplement (Gibco, USA), with medium half changes every 2−3 days. At 3 days in vitro (DIV), AraC (0.002 mM, Sigma-Aldrich, USA) was introduced to selectively inhibit astrocyte proliferation. Cultured neurons were transfected with 1 μg per well of the pAAV-AscI-CAG-NES-NeIle-L3-mCherry and pAAV-AscI-CAG-dMito2-NeIle-L3-mCherry plasmids at 5 DIV using a commercial calcium phosphate kit (Invitrogen, USA) following the manufacturer's protocol. After a 40 min incubation with calcium phosphate precipitate, the wells were washed with acidic MEM buffer (pH 6.6−6.7) to eliminate residual precipitates. Imaging of neurons and astrocytes was conducted between DIV11 and DIV13 using the CSU-W1 SoRa imaging setup of Nikon Spinning-Disk Field Scanning Confocal System with 488 and 561 nm excitation lasers under 40× NA1.15 objective lens (Nikon, Japan).

Protein Crystallization. An initial crystallization screening of Nelle was performed with a robotic crystallization system (Rigaku, Woodlands, TX, USA) and commercially available 96-well crystallization screens (Hampton Research, Aliso Viejo, CA, USA and Anatrace, Maumee, OH, USA) at 15 °C by using the sitting drop vapor diffusion method. The protein concentration was 10.0 mg/mL in the following buffer: 20 mM Tris, 10 mM isoleucine, and 150 mM NaCl pH 7.5. The hanging-drop vapor-diffusion method optimized the initial conditions in 24−4 Intelli plates. The crystals were obtained within several days under the following conditions: 18% PEG3350, 0.2 M Sodium acetate trihydrate pH 7.0.

Data Collection, Structure Solution, and Refinement. Crystals were briefly soaked in a cryosolution containing precipitant supplemented with 25% Glycerol (Hampton Research, Aliso Viejo, CA, USA) immediately prior to flash-frozen in liquid nitrogen and diffraction data collection. Diffraction data were collected at the home source Rigaku XtaLAB Synergy-S laboratory system to 2.65 Å resolution (The Woodlands, Texas, USA) and processed and merged using the CrysAlis software [Rigaku OD CrysAlis PRO; Rigaku Oxford Diffraction: Yarnton, UK, 2019]. The structure of Nelle was solved using MOLREP program[19] with PDB 5LTP and 1Z18 as a model. Refinement was carried out using the REFMAC5 program of the CCP4 suite.[20] To increase structure quality, data collection was performed at BL18U1 beamline of the SSRF (Shinghi, China). The structure was solved at 1.62 Å resolution using a 2.65 Å structure as the initial model and refined using the same programs. The visual inspection of electron density maps and the manual rebuilding of the model were carried out using the COOT interactive graphics program. Linkers between the LIVBP isoleucine-binding domain and fluorescent domain were built manually using the Coot program. Data collection and refinement statistics are summarized in Table S3. The asymmetric unit of the structure contains one molecule. Region 104-126 is not visible in the electron density map and is not included in the final model.

Statistical Processing of the Results. Figures represent mean values ± standard error throughout. For the comparison of two groups, an unpaired Mann−Whitney's *t*-test was used. All statistical analyses were performed using GraphPad Prism 6. Differences between groups are denoted as ns for not significant, * for $P < 0.05$, ** for $P < 0.01$, *** for $P < 0.001$, and **** for $P < 0.0001$.

Reporting Summary. Further information on research design is available in the Nature Portfolio Reporting Summary linked to this article.

CONCLUSIONS

For the first time, we developed a genetically encoded intensiometric green fluorescent indicator for BCAAs (isoleucine, leucine, and valine), NeIle, which allows for detection of the isoleucine amino acid and with lower dynamic range leucine and valine in vitro. NeIle has good localization and expression levels in different organelles of mammalian cells. Using a ratiometric version of the NeIle sensor, we successfully determined relative total concentrations of the BCAA (relying on relative green-to-red ratios) and studied the dynamics of isoleucine transients in different organelles of the mammalian cells. Finally, we analyzed the X-ray crystal structure of the NeIle indicator and generated structure-guided prototypes with an inverted fluorescence response and different selectivity to isoleucine, leucine, and valine amino acids. We anticipate that the NeIle indicator will boost the understanding of the role of the BCAAs in the nervous system and facilitate the development of industrial super producing strains.

ASSOCIATED CONTENT

Data Availability Statement

The plasmids used in this study are available from WeKwikGene (https://wekwikgene.wllsb.edu.cn/). All the experimental data are available upon request from the corresponding authors.

Supporting Information

The Supporting Information is available free of charge at https://pubs.acs.org/doi/10.1021/acssensors.4c01055.

Additional characteristics of NeIle mutants, list of primers, crystallographic data statistics, desing of sensors, localization and relative brightness of NeIle in HeLa cells, structural comparison of NeIle with LIVBP and mNeonGreen proteins, and nucleotide sequence of LIVBP (PDF)

AUTHOR INFORMATION

Corresponding Authors

Kiryl D. Piatkevich − *School of Life Sciences, Westlake University, Hangzhou 310024, China; Westlake Laboratory of Life Sciences and Biomedicine, Hangzhou 310024, China; Institute of Basic Medical Sciences, Westlake Institute for Advanced Study, Hangzhou 310024, China;* orcid.org/

https://doi.org/10.1021/acssensors.4c01055
ACS Sens. 2024, 9, 5135−5147

0000-0002-7777-9468; Email: kiryl.piatkevich@westlake.edu.cn

Fedor V. Subach − *Complex of NBICS Technologies, National Research Center "Kurchatov Institute", Moscow 123182, Russia;* orcid.org/0000-0003-2720-7821; Email: subach_fv@nrcki.ru

Authors

Aysilu N. Asanova − *Complex of NBICS Technologies, National Research Center "Kurchatov Institute", Moscow 123182, Russia*

Oksana M. Subach − *Complex of NBICS Technologies, National Research Center "Kurchatov Institute", Moscow 123182, Russia*

Sofya A. Myachina − *Complex of NBICS Technologies, National Research Center "Kurchatov Institute", Moscow 123182, Russia*

Marta A. Evteeva − *Complex of NBICS Technologies, National Research Center "Kurchatov Institute", Moscow 123182, Russia*

Natalia M. Gunitseva − *Complex of NBICS Technologies, National Research Center "Kurchatov Institute", Moscow 123182, Russia*

Anna A. Borisova − *Complex of NBICS Technologies, National Research Center "Kurchatov Institute", Moscow 123182, Russia*

Maksim V. Patrushev − *Complex of NBICS Technologies, National Research Center "Kurchatov Institute", Moscow 123182, Russia*

Anna V. Vlaskina − *Complex of NBICS Technologies, National Research Center "Kurchatov Institute", Moscow 123182, Russia*

Alena Yu. Nikolaeva − *Complex of NBICS Technologies, National Research Center "Kurchatov Institute", Moscow 123182, Russia;* orcid.org/0000-0003-4255-5170

Lina Yang − *School of Life Sciences, Westlake University, Hangzhou 310024, China; Westlake Laboratory of Life Sciences and Biomedicine, Hangzhou 310024, China; Institute of Basic Medical Sciences, Westlake Institute for Advanced Study, Hangzhou 310024, China*

Azat Gabdulkhakov − *Institute of Protein Research, Russian Academy of Sciences, Pushchino 142290, Russia;* orcid.org/0000-0003-1016-5936

Elizaveta Dronova − *Moscow Insitite of Physics and Technology, Dolgoprudny 141700, Russia*

Valeriya R. Samygina − *Complex of NBICS Technologies, National Research Center "Kurchatov Institute", Moscow 123182, Russia;* orcid.org/0000-0002-1528-5972

Xian Xiao − *School of Life Sciences, Westlake University, Hangzhou 310024, China; Westlake Laboratory of Life Sciences and Biomedicine, Hangzhou 310024, China; Institute of Basic Medical Sciences, Westlake Institute for Advanced Study, Hangzhou 310024, China*

Hu Zhao − *Chinese Institute for Brain Research, Beijing 102206, China*

Complete contact information is available at: https://pubs.acs.org/10.1021/acssensors.4c01055

Author Contributions

A.N.A., O.M.S., S.A.M., M.A.E., N.M.G., and A.A.B. developed the NeIle sensor, O.M.S. and S.A.M. characterized NeIle sensor in vitro, A.V.V. purified the NeIle protein, A.Yu.N. performed crystallization, A.G. performed X-ray data collection, V.R.S. performed crystallization, structure solution, refinement, and analysis, F.V.S. characterized the NeIle sensor in HeLa cells, L.Y., X.X, H.Z., and K.D.P. characterized the NeIle sensor in astrocytes and neurons, and F.V.S. and O.M.S. wrote the manuscript. All authors reviewed the manuscript.

Notes

Ethics statement: This article does not contain any studies involving humans and mammalians as subjects.

The authors declare no competing financial interest.

■ ACKNOWLEDGMENTS

The work was carried out within the state assignment of NRC "Kurchatov Institute" (development of NeIle), by the Ministry of Science and Higher Education of the Russian Federation for the development of the Kurchatov Center for Genome Research 075-15-2019-1659 (NeIle protein purification) and supported in part by start-up funding from the Foundation of Westlake University, Westlake Laboratory of Life Sciences and Biomedicine, National Natural Science Foundation of China grant 32171093 and "Pioneer" and "Leading Goose" R&D Program of Zhejiang 2024SSYS0031 to K.D.P., and a startup fund from the Chinese Institute for Brain Research to H.Z. (characterized NeIle sensor in astrocytes and neurons). The work was also supported by the Resource Centers department of the National Research Center Kurchatov Institute (imaging of bacteria).

■ ABBREVIATIONS

FP, fluorescent protein
GEAI, genetically encoded amino acid indicators
GFP, green fluorescent protein
FRET, Förster resonance energy transfer
PBS, phosphate-salt buffer
FPLC, fast protein liquid chromatography
PCR, polymerase chain reaction
QY, quantum yield

■ REFERENCES

(1) Dalangin, R.; Kim, A.; Campbell, R. E. The Role of Amino Acids in Neurotransmission and Fluorescent Tools for Their Detection. *Int. J. Mol. Sci.* **2020**, *21* (17), 6197.

(2) Dullius, A.; Fassina, P.; Giroldi, M.; Goettert, M. I.; Volken de Souza, C. F. A biotechnological approach for the production of Branched-chain amino acid containing bioactive peptides to improve human health: A review. *Food Res. Int.* **2020**, *131*, 109002.

(3) Becker, J.; Wittmann, C. Systems and synthetic metabolic engineering for amino acid production - the heartbeat of industrial strain development. *Curr. Opin. Biotechnol.* **2012**, *23* (5), 718−726.

(4) Shimomura, Y.; Kitaura, Y. Physiological and pathological roles of branched-chain amino acids in the regulation of protein and energy metabolism and neurological functions. *Pharmacol. Res.* **2018**, *133*, 215−217.

(5) Singh, S.; Sharma, M. P.; Alqarawi, A. A.; Hashem, A.; Abd_Allah, E. F.; Ahmad, A. Real-Time Optical Detection of Isoleucine in Living Cells through a Genetically-Encoded Nanosensor. *Sensors* **2019**, *20* (1), 146.

(6) Okada, S.; Ota, K.; Ito, T. Circular permutation of ligand-binding module improves dynamic range of genetically encoded FRET-based nanosensor. *Protein Sci.* **2009**, *18* (12), 2518−2527.

(7) Yoshida, T.; Nakajima, H.; Takahashi, S.; Kakizuka, A.; Imamura, H. OLIVe: A Genetically Encoded Fluorescent Biosensor for Quantitative Imaging of Branched-Chain Amino Acid Levels inside Single Living Cells. *ACS Sens.* **2019**, *4* (12), 3333−3342.

(8) Nasu, Y.; Shen, Y.; Kramer, L.; Campbell, R. E. Structure- and mechanism-guided design of single fluorescent protein-based biosensors. *Nat. Chem. Biol.* **2021**, *17* (5), 509−518.
(9) Piatkevich, K. D.; Murdock, M. H.; Subach, F. V. Advances in Engineering and Application of Optogenetic Indicators for Neuroscience. *Appl. Sci.* **2019**, *9* (3), 562.
(10) Zhang, Y.; Rózsa, M.; Liang, Y.; Bushey, D.; Wei, Z.; Zheng, J.; Reep, D.; Broussard, G. J.; Tsang, A.; Tsegaye, G.; et al. Fast and sensitive GCaMP calcium indicators for imaging neural populations. *Nature* **2023**, *615* (7954), 884−891.
(11) Barykina, N. V.; Subach, O. M.; Doronin, D. A.; Sotskov, V. P.; Roshchina, M. A.; Kunitsyna, T. A.; Malyshev, A. Y.; Smirnov, I. V.; Azieva, A. M.; Sokolov, I. S.; et al. A new design for a green calcium indicator with a smaller size and a reduced number of calcium-binding sites. *Sci. Rep.* **2016**, *6*, 34447.
(12) Subach, O. M.; Sotskov, V. P.; Plusnin, V. V.; Gruzdeva, A. M.; Barykina, N. V.; Ivashkina, O. I.; Anokhin, K. V.; Nikolaeva, A. Y.; Korzhenevskiy, D. A.; Vlaskina, A. V.; et al. Novel Genetically Encoded Bright Positive Calcium Indicator NCaMP7 Based on the mNeonGreen Fluorescent Protein. *Int. J. Mol. Sci.* **2020**, *21* (5), 1644.
(13) Trakhanov, S.; Vyas, N. K.; Luecke, H.; Kristensen, D. M.; Ma, J.; Quiocho, F. A. Ligand-free and -bound structures of the binding protein (LivJ) of the Escherichia coli ABC leucine/isoleucine/valine transport system: trajectory and dynamics of the interdomain rotation and ligand specificity. *Biochemistry* **2005**, *44* (17), 6597−6608.
(14) Oltrogge, L. M.; Wang, Q.; Boxer, S. G. Ground-state proton transfer kinetics in green fluorescent protein. *Biochemistry* **2014**, *53* (37), 5947−5957.
(15) Proksch, E. pH in nature, humans and skin. *J. Dermatol.* **2018**, *45* (9), 1044−1052.
(16) Chen, T. W.; Wardill, T. J.; Sun, Y.; Pulver, S. R.; Renninger, S. L.; Baohan, A.; Schreiter, E. R.; Kerr, R. A.; Orger, M. B.; Jayaraman, V.; et al. Ultrasensitive fluorescent proteins for imaging neuronal activity. *Nature* **2013**, *499* (7458), 295−300.
(17) Subach, O. M.; Barykina, N. V.; Chefanova, E. S.; Vlaskina, A. V.; Sotskov, V. P.; Ivashkina, O. I.; Anokhin, K. V.; Subach, F. V. FRCaMP, a Red Fluorescent Genetically Encoded Calcium Indicator Based on Calmodulin from Schizosaccharomyces Pombe Fungus. *Int. J. Mol. Sci.* **2021**, *22* (1), 111.
(18) Gauthier-Coles, G.; Vennitti, J.; Zhang, Z.; Comb, W. C.; Xing, S.; Javed, K.; Bröer, A.; Bröer, S. Quantitative modelling of amino acid transport and homeostasis in mammalian cells. *Nat. Commun.* **2021**, *12* (1), 5282.
(19) Vagin, A.; Teplyakov, A. MOLREP: an automated program for molecular replacement. *J. Appl. Crystallogr.* **1997**, *30* (6), 1022−1025.
(20) Collaborative Computational Project, Number 4. The CCP4 suite: programs for protein crystallography. *Acta Crystallogr., Sect. D: Biol. Crystallogr.* **1994**, *50* (5), 760.
(21) Subach, O. M.; Cranfill, P. J.; Davidson, M. W.; Verkhusha, V. V. An enhanced monomeric blue fluorescent protein with the high chemical stability of the chromophore. *PLoS One* **2011**, *6* (12), No. e28674.

https://doi.org/10.1021/acssensors.4c01055
ACS Sens. 2024, 9, 5135−5147